Transaction A: Civil Engineering
Vol. 17, No. 2, pp. 141–160

SCIENTIA IRANICA

Modeling of Moving Boundaries in Large Plasticity Deformations via an Enriched Arbitrary Lagrangian-Eulerian FE Method

M. Anahid[1] and A.R. Khoei[2,*]

Abstract. *In this paper, a new computational technique is presented for the modeling of moving boundaries in large plastic deformations based on an enriched arbitrary Lagrangian-Eulerian finite element method. An Arbitrary Lagrangian-Eulerian (ALE) technique is employed to capture the advantages of both Lagrangian and Eulerian methods and alleviate the drawbacks of mesh distortion in Lagrangian formulation. An enriched finite element method is implemented based on the extended FEM technique to capture the arbitrary interfaces independent of element boundaries. The process is accomplished by performing a splitting operator to separate the material (Lagrangian) phase from the convective (Eulerian) phase, and partitioning the Lagrangian and relocated meshes with some sub-quadrilaterals whose Gauss points are used for integration of the domain of elements. In order to demonstrate the efficiency of the enriched ALE finite element model in large deformations, several numerical examples including the coining problem with horizontal and vertical moving boundaries and a tensile plate with a moving interface are presented and the results are compared with those of the standard finite element and extended finite element methods.*

Keywords: *Large plasticity deformations; Arbitrary Lagrangian-Eulerian; Enriched FEM; Partition of unity; Godunov technique.*

INTRODUCTION

In large deformation problems with discontinuities and material interfaces, the implementation of adaptive mesh refinement in different stages of analysis is of great importance. The requirement of adaptive mesh refinement may consume high amounts of capacity and time. Thus, it is necessary to perform an innovative procedure to alleviate these difficulties by allowing the discontinuities to be mesh-independent. The eXtended Finite Element Method (X-FEM) has been successfully applied to problems exhibiting discontinuities and inhomogeneities, such as cracks, holes, or material interfaces. In this technique, the discontinuities are taken into account by adding appropriate functions into the standard approximation through a partition of unity method [1]. The technique was first introduced by Dolbow [2], Belytschko and Black [3] and Moës et al. [4] to model cracks, voids and inhomogeneities. The method allows modeling the entire crack geometry independently of the mesh, and completely avoids the need to remesh as the crack grows. The X-FEM was used to model crack growth and arbitrary discontinuities by enriching the discontinuous approximation in terms of a signed distance and level sets functions [5-11]. The method was implemented in various solid and fluid mechanics problems including: the moving particles [12], microstructures with complex geometries [13], moving hyper-surface with arbitrary discontinuities in space-time [14,15], stationary and growing cracks [16], bimaterial interfacial cracks [17], simulation of strong and weak discontinuities [18,19], plasticity of frictional contact [20,21] and nonlinear analysis of pressure-sensitive materials [22-24].

A common feature of the large plastic deformation

1. *Department of Mechanical Engineering, The Ohio State University, Columbus, OH 43210 USA.*
2. *Center of Excellence in Structures and Earthquake Engineering, Department of Civil Engineering, Sharif University of Technology, Tehran, P.O. Box 11155-9313, Iran.*
*. *Corresponding author. E-mail: arkhoei@sharif.edu*

Received 5 January 2010; accepted 20 February 2010

analysis of solid mechanics problems is the use of a Lagrangian kinematics formulation. This approach has shown to be adequate for problems that do not exhibit large mass fluxes among different parts of the problem. However, in large deformation analysis, the conventional finite element and extended finite element techniques using the updated Lagrangian formulation may suffer from serious numerical difficulties when the deformation of material is significantly large. This difficulty can be particularly observed in higher order elements when severe distortion of elements may lead to singularities in the isoparametric mapping of the elements, aborting the calculations or causing numerical errors [25]. In order to solve this problem, the mesh adaptive strategy was incorporated in large deformation analysis [26,27], however, it is computationally expensive, and information must be interpolated from the old mesh to the new mesh. In order to overcome this difficulty, the Arbitrary Lagrangian-Eulerian (ALE) approach has been proposed by researchers for the classical finite element method. In the ALE approach, the mesh motion is taken arbitrarily from material deformation to keep element shapes optimal. The ALE formulation was first applied to nonlinear solid mechanics path-dependent materials with a definition of the tangent stiffness matrix and the consistent linearization process by Haber [28], Liu et al. [29,30] and Benson [31]. The technique was then implemented in various solid mechanics problems including: incompressible hyperelasticity [32], metal forming simulation [33-35], transient dynamic analysis [36], hyperelastoplasticity [37], finite strain plasticity [38,39] and pressure-sensitive materials [40,41]. A key issue in ALE formulation is an efficient mesh motion technique in order to achieve satisfactory results. There are various mesh relocation techniques based on the ALE split operator [31], a uniform distribution of the equivalent plastic strain indicator [33], the transfinite mapping algorithm using nodal relocation [34,35] etc. These techniques are able to keep elements with a good shape by equalizing the size of elements and by avoiding shape distortion without changing the mesh topology.

The aim of present study is to extend the X-ALE-FEM technique recently developed by authors in [42] to the large plastic deformation analysis of moving boundary problems. An enriched FE model is incorporated with the ALE technique in large plastic deformation based on an operator splitting technique. The constitutive equation of ALE nonlinear mechanics contains a convective term which reflects the relative motion between the physical motion and the mesh motion. The correct treatment of this convective term in the constitutive Equation is the key point in ALE nonlinear solid mechanics. The most popular approach in dealing with the convective term is the use of a split or fractional-step method. In fact, each time-step is first divided into a Lagrangian phase and an Eulerian phase. Convection is neglected in the material phase, which is, thus, identical to a time-step in a standard Lagrangian analysis. The stress and plastic internal variables are then transferred from Lagrangian mesh to the relocated mesh in order to evaluate relative mesh-material motion in the convection phase. Hence, in order to perform an enriched arbitrary Lagrangian-Eulerian FE analysis, a typical X-FEM analysis is first carried out in the Lagrangian phase using the updated Lagrangian approach. The Eulerian phase is then applied to update the mesh, while the material interface is independent of the FE mesh. Special care has to be taken with respect to the integration of constitutive Equations, often denoted as the stress update, since the stress field is usually discontinuous across the elements due to the fact that stress values are only evaluated at discrete integration points. To handle this, an approach called the Godunov scheme is used here for the stress update. This uncoupled approach makes easy the extension of a pure extended Lagrangian FE code to the ALE technique and allows the use of the original updated Lagrangian program to solve the relevant ALE equations.

The plan of the paper is as follows: The X-FEM technique is briefly presented in the next section. The arbitrary Lagrangian-Eulerian method is then introduced in large deformation problems. The algorithm of the uncoupled ALE solution together with the mesh motion strategy and stress update procedure are demonstrated based on the Godunov method for the transferring of variables from Lagrangian mesh to relocated mesh. An enriched ALE finite element technique is described based on the combined ALE and X-FEM methods to reduce the mesh distortion occurred in conventional large X-FEM deformation. A technique is presented in this section to update the nodal values of a level set and stress components during the Eulerian phase. Finally, the numerical simulation of several examples is presented to demonstrate the capability of the X-ALE-FEM technique in large plastic deformation problems.

AN ENRICHED FINITE ELEMENT METHOD

The enriched finite element method is a powerful and accurate approach to model discontinuities, which are independent of the FE mesh topology. In this technique, the discontinuities or interfaces are not considered in the mesh generation operation, and special functions, which depend on the nature of discontinuity, are included into the finite element approximation. The aim of this method is to simulate the discontinuity, or interface, with minimum enrichment. In X-FEM, the enrichment functions are associated with new degrees

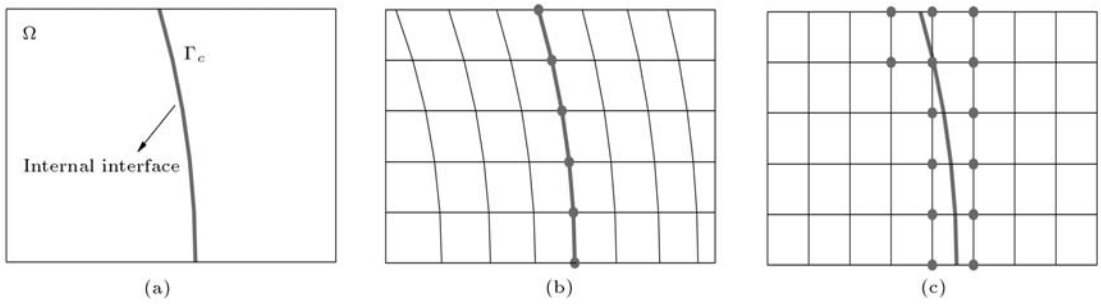

Figure 1. Modeling of internal interfaces; a) Problem definition, b) The FE mesh which conforms to the geometry of discontinuity, c) A uniform mesh in which the circled nodes have additional degrees of freedom and enrichment functions.

of freedom and approximation of the displacement field, described in Figure 1 as:

$$\mathbf{u}(\mathbf{x}) = \sum_I N_I(\mathbf{x})\bar{\mathbf{u}}_I + \sum_J N_J(\mathbf{x})\psi(\mathbf{x})\mathbf{a}_J,$$

$$\text{for} \quad n_I \in \mathbf{n}_T \quad \text{and} \quad n_J \in \mathbf{n}_e. \tag{1}$$

The first term of the above equation denotes the classical finite element approximation and the second term indicates the enrichment function considered in X-FEM. In this equation, $\bar{\mathbf{u}}_I$ is the classical nodal displacement; $\mathbf{a}_J$, the nodal degrees of freedom corresponding to the enrichment functions; $\psi(\mathbf{x})$, the enrichment function, and $N(\mathbf{x})$, the standard shape function. In Equation 1, $\mathbf{n}_T$ represents the set of all nodes of the global domain, and $\mathbf{n}_e$ the set of nodes of elements split by the interface, as indicated in Figure 1c.

The choice of enrichment functions in displacement approximation is dependent on the conditions of the problem. The *level set method* is a numerical scheme developed by Sethian [43] for tracking the motion of interfaces. This method, which is used for predicting the geometry of boundaries, is very suitable for bi-material problems, in which the displacement field is continuous but there is a jump in the strain field. In this technique, the interface is implicitly represented by assigning a level set value to node I of the mesh, located at distance φ_I from the interface. The sign of its value is negative on one side and positive on the other. The level set function can be then obtained with interpolating the nodal values using standard FE shape functions as:

$$\varphi(\mathbf{x}) = \sum_I \varphi_I N_I(\mathbf{x}), \tag{2}$$

where the above statement indicates the summation over the nodes, which belong to elements cut by the interface. A discontinuity is represented by the zero value of level set φ. The new degrees of freedom, $\mathbf{a}_J$, corresponding to the level set enrichment function are considered in Equation 1 in order to attribute to the nodes that belong to the set of $\mathbf{n}_e$. In order to improve the numerical computation in X-FEM, it is preferable to have a uniform distribution of shape functions around the boundary of discontinuity. To this goal, a technique for smoothing the values of the level set is applied by employing the nodes that belong to the elements in the neighborhood of discontinuity elements. Sukumar et al. [6] proposed the absolute value of the level set function to implement the enrichment function in the modeling of discontinuity as a result of different types of material properties. This function has a discontinuous first derivative on the interface defined as:

$$\psi^1(\mathbf{x}) = \left|\sum_I \varphi_I N_I(\mathbf{x})\right|. \tag{3}$$

An extension of the above function was proposed by Moës et al. [13] that improves the previous enrichment strategy, and has the convergence rate very close to the optimal FE convergence. The modified level set function has a ridge centered on the interface and zero value on the elements that are not crossed by the interface. This level set function, ψ^2, is defined as:

$$\psi^2(\mathbf{x}) = \sum_I |\varphi_I| N_I(\mathbf{x}) - \left|\sum_I \varphi_I N_I(\mathbf{x})\right|. \tag{4}$$

Considering the enriched approximation of the displacement field defined by Equation 1, the value of $\mathbf{u}(\mathbf{x})$ on an enriched node, K, in set $\mathbf{n}_e$, can be written as:

$$\mathbf{u}(\mathbf{x}_K) = \bar{\mathbf{u}}_K + \psi(\mathbf{x}_K)\mathbf{a}_K. \tag{5}$$

Since $\psi(\mathbf{x}_K)$ is not necessarily zero, the above expression is not equal to the real nodal value, $\bar{\mathbf{u}}_K$. Thus, the enriched displacement field (1) can be corrected as:

$$\mathbf{u}(\mathbf{x}) = \sum_I N_I(\mathbf{x})\bar{\mathbf{u}}_I + \sum_J N_J(\mathbf{x})(\psi(\mathbf{x}) - \psi(\mathbf{x}_J))\mathbf{a}_J,$$

$$\text{for} \quad n_I \in \mathbf{n}_T \quad \text{and} \quad n_J \in \mathbf{n}_e. \tag{6}$$

Based on the new definition in the last term of Relation 6, the expected property can be obtained as $\mathbf{u}(\mathbf{x}_K) = \bar{\mathbf{u}}_K$. Using the enrichment function, $\psi(\mathbf{x})$, based on its nodal values as $\psi(\mathbf{x}) = \sum_I N_I(\mathbf{x})\psi_I$, Equation 6 can be rewritten as:

$$\mathbf{u}(x) = \sum_I N_I(\mathbf{x})\bar{\mathbf{u}}_I + \sum_J \left(N_J(\mathbf{x}) \left(\sum_K N_K(\mathbf{x})\psi_K - \psi_J \right) \mathbf{a}_J \right). \quad (7)$$

It must be noted that the numerical integration of the weak form with the standard Gauss quadrature points for elements cut by the interface must be improved because of the existence of a discontinuous displacement gradient through the interface.

ARBITRARY LAGRANGIAN-EULERIAN FORMULATION

In the ALE description, the choice of the material, spatial or any arbitrary configuration yields to a Lagrangian, Eulerian or arbitrary Lagrangian-Eulerian description, respectively. In this method, since the mesh motion is taken arbitrarily from material deformation to keep element shapes optimal, the convective term appears in the balance of momentum equation. The main difficulty in extending the ALE formulation from FEM to X-FEM is the convective term, which reflects the relative motion between the physical motion and the mesh motion. The correct treatment of this convective term in X-FEM is the key point in the X-ALE-FEM modeling of solid mechanic problems. The most popular approach in dealing with the convective term is the use of a split or fractional-step method. Each time-step is divided into a Lagrangian phase and an Eulerian phase. Convection is neglected in the material phase, which is, thus, identical to a time-step in a standard Lagrangian X-FEM analysis. The stress and plastic internal variables are then transferred from Lagrangian mesh to the relocated mesh in order to evaluate the relative mesh-material motion in the convection phase. Special care has to be taken with respect to the time integration of the constitutive equations, often denoted as the stress update, since the stress field is usually discontinuous across the elements due to the fact that stress values are only evaluated at discrete integration points that normally lie inside the element. To handle this, an approach called the Godunov scheme is used here for the stress update.

Kinematics

In the ALE description, three different configurations are considered: the material domain, Ω_0, spatial domain, Ω, and reference domain, $\hat{\Omega}$, which is called the ALE domain. The material motion is defined by $x_i^m = f_i(X_j, t)$, with X_j denoting the material point coordinates and $f_i(X_j, t)$ a function that maps the body from the initial or material configuration, Ω_0, to the current or spatial configuration, Ω. The initial position of material points is denoted by x_i^g, called the reference or ALE coordinate in which $x_i^g = f_i(X_j, 0)$. The reference domain, $\hat{\Omega}$, is defined to describe the mesh motion and is coincident with mesh points so it can be denoted by the computational domain. The mesh motion is defined by $x_i^m = \hat{f}_i(x_j^g, t)$. The material coordinate can be then related to the ALE coordinate by $x_i^g = \hat{f}_i^{-1}(x_j^m, t)$. The mesh displacement can be defined by:

$$u_i^g(x_j^g, t) = x_i^m - x_i^g = \hat{f}_i(x_j^g, t) - x_i^g. \quad (8)$$

It must be noted that mesh motion can be simply obtained from material motion replacing the material coordinate by the ALE coordinate. The mesh velocity can be defined as:

$$v_i^g(x_j^g, t) = \frac{\partial \hat{f}_i(x_j^g, t)}{\partial t} = \left.\frac{\partial x_i^m}{\partial t}\right|_{x_j^g}, \quad (9)$$

in which the ALE coordinate, x_j^g, and material coordinate, X_j, in the material velocity are fixed. In ALE formulation, the convective velocity, c_i, is defined using the difference between the material and mesh velocities as:

$$c_i = v_i^m - v_i^g = \left.\frac{\partial x_i^m}{\partial x_j^g}\,\frac{\partial x_j^g}{\partial t}\right|_{X_k} = \frac{\partial x_i^m}{\partial x_j^g} w_j, \quad (10)$$

where the material velocity, $v_i^m = (\partial x_i^m/\partial t)_{X_j}$, can be obtained using the chain rule expression with respect to the ALE coordinate, x_j^g, and time, t. In Equation 10, the referential velocity, w_i, is defined by $w_i = (\partial x_i^g/\partial t)_{X_j}$. The above relationship between the convective velocity, c_i, material velocity, v_i^m, mesh velocity, v_i^g, and referential velocity, w_i, is frequently used in ALE formulation.

Now, the general relationship between material time derivatives and referential time derivatives of any scalar function, f_i, can be written as:

$$\left.\frac{\partial f_i}{\partial t}\right|_{X_j} = \left.\frac{\partial f_i}{\partial t}\right|_{x_j^g} + \frac{\partial f_i}{\partial x_i^g}\left.\frac{\partial f_i}{\partial t}\right|_{X_j} = \left.\frac{\partial f_i}{\partial t}\right|_{x_j^g} + \frac{\partial f_i}{\partial x_j^m} c_j. \quad (11)$$

The above equation can be used to deduce the fundamental conservation laws of continuum mechanics, i.e. the momentum, mass and constitutive equations, in a nonlinear ALE description.

Governing Equations

In the ALE technique, the governing equations can be derived by substituting the relationship between the material time derivatives and referential time derivatives, i.e. Equation 11, into the continuum mechanics governing equations. This substitution gives rise to convective terms in the ALE equations, which account for the transport of material through the grid. Thus, the momentum equation in ALE formulation can be written similar to the updated Lagrangian description by consideration of the material time derivative terms, as:

$$\rho \dot{v}_i^m = \sigma_{ji,j} + \rho b_i, \tag{12}$$

where ρ is the density, σ the Cauchy stress and b_i the body force. In the above equation, the material time derivative of velocity $\dot{v}_i^m$ can be obtained by specializing the general Relationship 11 to $\dot{v}_i^m$, as:

$$\dot{v}_i^m = \left.\frac{\partial v_i^m}{\partial t}\right|_{x_j^g} + \frac{\partial v_i^m}{\partial x_j^m} c_j. \tag{13}$$

Substituting Equation 13 into 12, the momentum equation can be then written as:

$$\rho \left(\left.\frac{\partial v_i^m}{\partial t}\right|_{x_j^g} + \frac{\partial v_i^m}{\partial x_j^m} c_j \right) = \frac{\partial \sigma_{ij}}{\partial x_j^m} + \rho b_i. \tag{14}$$

The mass balance in ALE formulation can be similarly derived by specializing the general Relationship 11 to the density, ρ, as:

$$\left.\frac{\partial \rho}{\partial t}\right|_{x_j^g} + \frac{\partial \rho}{\partial x_j^m} c_j = -\rho \left.\frac{\partial v_j^m}{\partial x_j^m}\right|_{X_j}. \tag{15}$$

Finally, in order to describe the constitutive equation for nonlinear ALE formulation, the general Relationship 11 is specialized to the stress tensor as:

$$\left.\frac{\partial \boldsymbol{\sigma}}{\partial t}\right|_{x_j^g} + \frac{\partial \boldsymbol{\sigma}}{\partial x_j^m} c_j = \mathbf{q}, \tag{16}$$

where $\mathbf{q}$ accounts for both the pure straining of the material and the rotational terms that counteract the non-objectivity of the material stress rate [36].

The basis of any mechanical initial boundary value problem in the framework of the material description is the balance of momentum equation. In the framework of the referential configuration, we have also considered mass balance and the constitutive equations, which are defined as partial differential equations in the case of the referential description. In the quasi-static problems, the inertia force, $\rho\mathbf{a}$, is negligible with respect to other forces of momentum equations, hence, the equilibrium equation in ALE and Lagrangian descriptions is exactly identical. In addition, considering the constant value of density, ρ, the balance of the mass equation results in $\partial v_j^m / \partial x_j^m | X_j = 0$, which is already satisfied. Thus, the governing equations of ALE formulation for quasi-static problems can be summarized into Equations 14 and 16.

Weak Form of ALE Formulation

In order to present the weak form of initial boundary value problems in the ALE description, the mass balance and the balance of linear momentum can be written in the integral form over the spatial domain, Ω, multiplied by the test functions, $\delta\rho$, $\delta\mathbf{v}$ and $\delta\boldsymbol{\sigma}$. Clearly, there must be a relationship between the strong and weak form of governing equations, in which these two forms are identical. The weak form of a momentum equation is obtained by multiplying the strong form of Equation 14 by the test function, $\delta\mathbf{v} \in U^0$, where $U^0 = \{\delta\mathbf{v} | \delta\mathbf{v} \in C^0,\ \delta\mathbf{v} = \mathbf{0} \text{ on } \Gamma_v\}$ and Γ_v indicates the part of the boundary in which the velocities are prescribed. Consider that $\mathbf{v} \in U$ is the trial solution with $U = \{\mathbf{v} | \mathbf{v} \in C^0,\ \mathbf{v} = \hat{\mathbf{v}} \text{ on } \Gamma_v\}$, and $\hat{\mathbf{v}}$ is the prescribed velocities in Γ_v, the integration over the spatial domain results in:

$$\int_\Omega \delta\mathbf{v}\rho \left(\left.\frac{\partial \mathbf{v}^m}{\partial t}\right|_{x^g} + \frac{\partial \mathbf{v}^m}{\partial \mathbf{x}^m}\mathbf{c} \right) dv = \int_\Omega \delta\mathbf{v}(\mathrm{div}_{x^m}\boldsymbol{\sigma} + \rho\mathbf{b}) dv, \tag{17}$$

or:

$$\int_\Omega \delta\mathbf{v}\rho \left.\frac{\partial \mathbf{v}^m}{\partial t}\right|_{\mathbf{x}^g} dv + \int_\Omega \delta\mathbf{v}\rho \frac{\partial \mathbf{v}^m}{\partial \mathbf{x}^m}\mathbf{c}\, dv = \int_\Omega \delta\mathbf{v}\ \mathrm{div}_{x^m}\boldsymbol{\sigma}\ dv + \int_\Omega \delta\mathbf{v}\ \rho\mathbf{b}\ dv. \tag{18}$$

To eliminate the stress derivatives, the first term of the right hand side in the above equation is rewritten using the integration, part by part, as:

$$\int_\Omega \delta\mathbf{v}\rho \left.\frac{\partial \mathbf{v}^m}{\partial t}\right|_{x^g} dv + \int_\Omega \delta\mathbf{v}\ \rho \frac{\partial \mathbf{v}^m}{\partial \mathbf{x}^m}\ \mathbf{c} dv = -\int_\Omega \mathrm{div}_{x^m}\ \delta\mathbf{v}\ \boldsymbol{\sigma}\ dv + \int_\Omega \delta\mathbf{v}\ \rho\mathbf{b}\ dv + \int_{\Gamma_t} \delta\mathbf{v}\ \hat{\mathbf{t}}\ d\Gamma, \tag{19}$$

where Γ_t refers to the part of the boundary in which the traction vector, $\hat{\mathbf{t}}$, is prescribed.

Since the mass balance is enforced in the referential description as a partial differential equation, a weak form must be developed. Considering the trial solution as $\rho \in C^0$, the weak form of the balance of mass can be obtained by integration of the strong form

of the mass balance, as given in Equation 15, over the spatial domain, Ω, which has been multiplied by a test function, $\delta\rho \in C^0$, as:

$$\int_{\Omega} \delta\rho \left(\frac{\partial \rho}{\partial t}\bigg|_{\mathbf{x}^g} + \frac{\partial \rho}{\partial \mathbf{x}^m}\mathbf{c} + \rho \frac{\partial \mathbf{v}^m}{\partial \mathbf{x}^m}\bigg|_{X} \right) dv = 0. \tag{20}$$

In this equation, only the first derivatives are appeared, with respect to the mass density, ρ, and the velocity, $\mathbf{v}$.

Similar to the momentum equation and mass balance, the weak form of the constitutive equation for nonlinear ALE formulation can be obtained by multiplying the strong form of Equation 16 with a test function, $\delta\boldsymbol{\sigma}$, and integrating over the spatial domain as:

$$\int_{\Omega} \delta\boldsymbol{\sigma} \left(\frac{\partial \boldsymbol{\sigma}}{\partial t}\bigg|_{x^g} + \frac{\partial \boldsymbol{\sigma}}{\partial \mathbf{x}^m}\mathbf{c} \right) dv = \int_{\Omega} \delta\boldsymbol{\sigma}\mathbf{q} dv, \tag{21}$$

or:

$$\int_{\Omega} \delta\boldsymbol{\sigma} \frac{\partial \boldsymbol{\sigma}}{\partial t}\bigg|_{x^g} dv + \int_{\Omega} \delta\boldsymbol{\sigma} \frac{\partial \boldsymbol{\sigma}}{\partial \mathbf{x}^m}\mathbf{c} dv = \int_{\Omega} \delta\boldsymbol{\sigma}\ \mathbf{q}\ dv. \tag{22}$$

ALE Finite Element Discretization

In the finite element method, the reference domain, Ω, is subdivided into a number of elements in which for each element, e, the ALE coordinates, $\mathbf{x}^g$, are defined as:

$$\mathbf{x}^g(\boldsymbol{\xi}) = \sum_{I=1}^{N^e} N_I(\boldsymbol{\xi})\mathbf{x}_I^g, \tag{23}$$

where $\boldsymbol{\xi}$ denotes the parent element coordinates, $N_I(\boldsymbol{\xi})$ is the interpolation shape function, $\mathbf{x}_I^g$ stands for the ALE coordinates of node I, and N^e is the number of nodes of element e. The mesh displacement field can be then written (following Equation 8) as:

$$\mathbf{u}^g(\boldsymbol{\xi}) = \mathbf{x}^m(\boldsymbol{\xi}) - \mathbf{x}^g(\boldsymbol{\xi}) = \sum_{I=1}^{N^e} N_I(\boldsymbol{\xi})\mathbf{u}_I^g. \tag{24}$$

Thus, the mesh, material and convective velocities can be defined:

$$\mathbf{v}^g(\boldsymbol{\xi}) = \frac{\partial \mathbf{x}^m}{\partial t}\bigg|_{x^g} = \sum_{I=1}^{N^e} N_I(\boldsymbol{\xi})\mathbf{v}_I^g,$$

$$\mathbf{v}^m(\boldsymbol{\xi}) = \frac{\partial \mathbf{x}^m}{\partial t}\bigg|_{X} = \sum_{I=1}^{N^e} N_I(\boldsymbol{\xi})\mathbf{v}_I^m,$$

$$\mathbf{c}(\boldsymbol{\xi}) = \mathbf{v}^m - \mathbf{v}^g = \sum_{I=1}^{N^e} N_I(\boldsymbol{\xi})(\mathbf{v}_I^m - \mathbf{v}_I^g)$$

$$= \sum_{I=1}^{N^e} N_I(\boldsymbol{\xi}^e)\mathbf{c}_I(t). \tag{25}$$

Furthermore, the internal variables, such as density and stress, can be approximated in the same manner as:

$$\rho(\boldsymbol{\xi}, t) = \sum_{I=1}^{N^e} N_I^{\rho}(\boldsymbol{\xi}^e)\rho^I(t),$$

$$\boldsymbol{\sigma}(\boldsymbol{\xi}, t) = \sum_{I=1}^{N^e} N_I^{\sigma}(\boldsymbol{\xi}^e)\boldsymbol{\sigma}^I(t), \tag{26}$$

where N_I^{ρ} and N_I^{σ} stand for the shape functions of density and stress, respectively. These shape functions may differ from those used to approximate the displacement field, N_I. It must be noted that because the convective terms appear in governing equations, the implementation of the standard Galerkin finite element formulation may result in numerical instabilities. This point is especially true for severe dynamic systems. One way to alleviate these difficulties is to employ the Petrov-Galerkin formulation. In this approach, different sets of shape function are used to interpolate the trial and test functions for displacement, stress and density.

Substituting the material and the convective velocity ($\mathbf{v}^m$ and $\mathbf{c}$), given in Equation 25, and the density and the stresses (ρ and $\boldsymbol{\sigma}$), given in Equation 26, into the weak form of the balance of linear momentum, given in Equation 18, yields to:

$$\mathbf{M}\frac{d\mathbf{v}^m}{dt} + \mathbf{L}\mathbf{v}^m + \mathbf{f}^{\text{int}} = \mathbf{f}^{\text{ext}}, \tag{27}$$

where:

$$\mathbf{M} = \int_{\Omega} \rho \mathbf{N}^T \mathbf{N} dv,$$

$$\mathbf{L} = \int_{\Omega} \rho \mathbf{N}^T \mathbf{c} \frac{d\mathbf{N}}{d\mathbf{x}^m} dv, \tag{28}$$

and:

$$\mathbf{f}^{\text{int}} = \int_{\Omega} \frac{d\mathbf{N}^T}{d\mathbf{x}^m}\boldsymbol{\sigma} dv,$$

$$\mathbf{f}^{\text{ext}} = \int_{\Omega} \rho \mathbf{N}^T \mathbf{b} dv + \int_{\Gamma} \mathbf{N}^T \hat{\mathbf{t}} d\Gamma. \tag{29}$$

As mentioned earlier, the term of inertia forces can be neglected in the quasi-static problems. Thus, the momentum Equation 27 can be simplified to $\mathbf{f}^{\text{int}} = \mathbf{f}^{\text{ext}}$.

In a similar manner, the FE formulation for the mass balance can be obtained by substituting the material velocity from Equation 25 and the density from Equation 26 into Equation 20 as:

$$\mathbf{M}^{\rho}\frac{d\rho}{dt}+\mathbf{L}^{\rho}\rho+\mathbf{K}^{\rho}\rho=\mathbf{0}, \tag{30}$$

where:

$$\mathbf{M}^{\rho}=\int_{\Omega}\mathbf{N}^{\rho^T}\mathbf{N}^{\rho}dv,$$

$$\mathbf{L}^{\rho}=\int_{\Omega}\mathbf{N}^{\rho^T}c\frac{d\mathbf{N}^{\rho}}{d\mathbf{x}^m}dv,$$

$$\mathbf{K}^{\rho}=\int_{\Omega}\mathbf{N}^{\rho^T}\mathrm{div}_{x^m}\mathbf{v}^m\mathbf{N}^{\rho}dv. \tag{31}$$

Finally, the FE formulation for the constitutive equation can be obtained by replacing the convective velocity from Equation 25 and the stresses from Equation 26 into Equation 22 as:

$$\mathbf{M}^{\sigma}\frac{d\boldsymbol{\sigma}}{dt}+\mathbf{L}^{T}\boldsymbol{\sigma}=\mathbf{q}, \tag{32}$$

where:

$$\mathbf{M}^{\sigma}=\int_{\Omega}\mathbf{N}^{\sigma^T}\mathbf{N}^{\sigma}dv,$$

$$\mathbf{L}^{\sigma}=\int_{\Omega}\mathbf{N}^{\sigma^T}\mathbf{c}\frac{d\mathbf{N}^{\sigma}}{d\mathbf{x}^m}dv. \tag{33}$$

UNCOUPLED ALE SOLUTION

There are, basically, two methods of solution for the governing equations of ALE Formulations 27, 30 and 32: the fully coupled solution and uncoupled solution [44]. In the fully coupled solution method, no further simplifications can be considered and various terms must be calculated simultaneously. This approach was used in the works of Yamada and Kikuchi [32], Bayoumi and Gadala [39] and Khoei et al. [40]. In the uncoupled solution technique, we do not consider the fully coupled equations and the whole process can be decoupled into a Lagrangian phase and an Eulerian phase by employing a splitting operator. Such a technique has been employed by Benson [31], Rodriguez-Ferran et al. [36] and Khoei et al. [41]. In an uncoupled technique, the analysis is first carried out according to the Lagrangian phase, at each time step until the required convergence is attained. The Eulerian phase is then applied to keep the mesh configuration regular. In this study, the uncoupled ALE solution is applied as it makes it possible to upgrade a standard Lagrangian X-FEM program to a X-ALE-FEM case with as little expenditure as possible. In this case, the Lagrangian computation can be included as a sub-step of the new ALE computation.

The basis of a splitting operator in an uncoupled solution is to separate the material (Lagrangian) phase from the convective (Eulerian) phase, which is combined with a smoothing phase (Figure 2). In the Lagrangian phase, the convective effects are neglected, so the material body deforms from its material configuration to its spatial one. In this framework, the nodal and quadrature points may lead eventually to a high distortion of the spatial discretization after the Lagrangian step. In order to reduce this distortion, a smoothing phase is then applied, which leads to the final spatial discretization. This allows computation of the mesh velocity, which leads to the convective velocity, or Eulerian phase. The advantage of the ALE splitting operator is that the calculations are performed in the Lagrangian step, with no convective terms, to achieve equilibrium. When equilibrium is achieved in the Lagrangian step, the Eulerian step is performed by transferring the internal variables from the Lagrangian mesh to the relocated mesh.

Material (Lagrangian) Phase

In the material phase, the convective terms are neglected, so, the momentum equation is identical to a time-step in a standard Lagrangian analysis. Thus, the momentum balance (Equation 27) in quasistatic analysis becomes:

$$\int_{\Omega}\frac{d\mathbf{N}^T}{d\mathbf{x}^m}\boldsymbol{\sigma}dv=\int_{\Omega}\rho\mathbf{N}^T\mathbf{b}dv+\int_{\Gamma}\mathbf{N}^T\hat{\mathbf{t}}d\Gamma, \tag{34}$$

which is a static equilibrium equation with no time, velocity and convective terms in the ALE momentum balance.

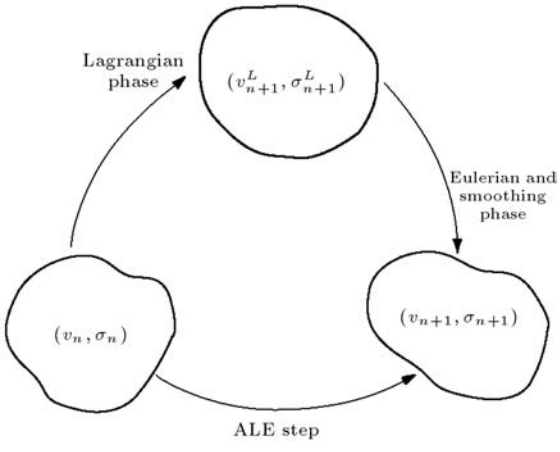

Figure 2. Decomposition of the ALE step into a Lagrangian phase and an Eulerian phase combined with a smoothing phase.

The ALE constitutive Equation 32 in the material phase can be simplified as:

$$\mathbf{M}^{\sigma}\frac{d\boldsymbol{\sigma}}{dt}=\mathbf{q}, \tag{35}$$

which needs to be integrated at each time step to update the stress from $\boldsymbol{\sigma}_n$ at time t_n to $\boldsymbol{\sigma}^L_{n+1}$ after the Lagrangian phase. It means that in the absence of convective terms, the grid points move together with material particles. Thus, the Lagrangian phase can be performed with the same stress update algorithm used in Lagrangian simulation, which handles the constitutive equation at the Gauss point level.

Smoothing Phase

In order to reduce the mesh distortion in spatial configuration, a remeshing procedure must be applied between the Lagrangian and the Eulerian phase. The algorithm can produce smoother meshes without redefining the element connectivity. Since the mesh moves independently from the material, we obtain the mesh velocity, which can be used to compute the convective velocity. There are various remeshing strategies that have been proposed by researchers [31,33-35]. In this study, the simple methods are used based on the 'Laplacian approach' and the 'mid-area averaging technique'. In these approaches, the mesh distortion is controlled by moving the inner nodes in an appropriate way. In addition, the boundary nodes are remained on the boundary by allowing only a tangential movement to those nodes.

The Laplacian approach is one of the most popular and simple smoothing strategies, which has been used by researchers to produce smoother meshes. In this technique, the spatial position of smoothed node, $\mathbf{x}_i$, can be computed using the spatial position after the Lagrangian phase, $\mathbf{x}^L_i$, as [45]:

$$\mathbf{x}_i=\frac{1}{(2-w)N}\sum_{e=1}^{N}\left(\mathbf{x}_{e1}+\mathbf{x}_{e2}-w\mathbf{x}_{e3}\right), \tag{36}$$

where $\mathbf{x}_i$ presents the spatial position of node i, and N is the number of four-node elements connecting to node i (typically $N=4$). For each element, $1\le e\le N$, $\mathbf{x}_{e1}$ and $\mathbf{x}_{e2}$ are the coordinates of the nodes of element e connected to $\mathbf{x}_i$ by an edge, and $\mathbf{x}_{e3}$ is the coordinate of the node of element e at the opposite corner of $\mathbf{x}_i$, as shown in Figure 3a. In the above relation, w is the weighting factor, $0\le w\le 1$, which, for $w=0$, yields to the commonly used Laplacian scheme [45].

The mid-area averaging technique is a modification of the Laplacian approach. In this method, the considered node is in the centroid of all connected elements, and the area of different elements is taken into account. Thus, the spatial position of smoothed node $\mathbf{x}_i$ can be computed as:

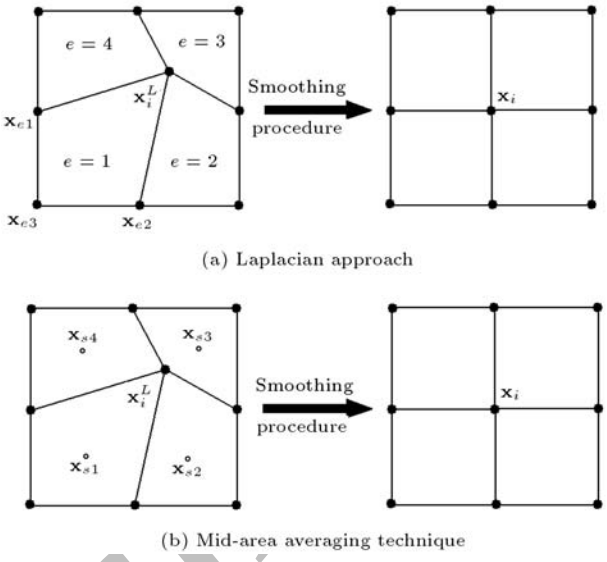

Figure 3. Remeshing procedure in smoothing phase.

$$\mathbf{x}_i=\frac{\sum_{e=1}^{N}A_e\mathbf{x}_{Se}}{\sum_{e=1}^{N}A_e}, \tag{37}$$

where $\mathbf{x}_{Se}$ is the location of the centroid of element e (Figure 3b), A_e is the area of element e and N indicates the number of four-node elements connecting to node i. After smoothing the position of all nodal points, $\mathbf{x}_{n+1}$, at time t_n, the convective term, $\mathbf{c}_{n+1}$, can be computed using the material (Lagrangian) displacement, $\mathbf{u}^L_{n+1}$, and mesh displacement, $\mathbf{u}^g_{n+1}$, for quasi-static problems, as $\mathbf{c}_{n+1}=\mathbf{u}^L_{n+1}-\mathbf{u}^g_{n+1}$.

In order to perform the smoothing procedure for boundary nodes, it is assumed that the nodal points remain on the boundary by allowing only a tangential movement to these nodes. In this case, the boundary nodes are allowed to move in a normal direction following the motion of the material points. For boundaries with a pre-known deformed shape, it is sufficient to assign a motion in the normal direction equal to the known material motion. To assign a desired tangential motion for nodal points, the following algorithm is performed here. First, a polynomial of second order is constructed using the considered node and two connected nodes on the boundary. The position of the mid-node is then corrected according to the position of two connected nodes as shown in Figure 4a. This procedure will not work properly when the determinant of the matrix of its solution becomes zero. To avoid this problem, the approach is modified in a manner whereby the extension of the mid-node lies on the next connecting line, as shown in Figure 4b.

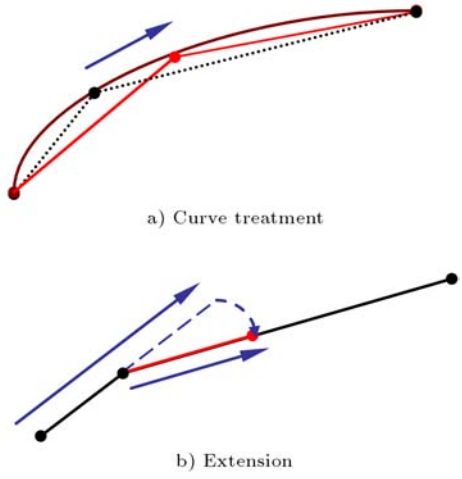

Figure 4. Illustration of boundaries motion.

Convection (Eulerian) Phase

The final part of the operator splitting technique includes the data transferring of the solution obtained by the Lagrangian phase onto the new relocated mesh, which was developed through the mesh smoothing algorithm. In the Eulerian (or convection) phase, the convective terms that were neglected during the Lagrangian phase are taken into account. Since we are dealing with history-dependent materials and due to the fact that different material integration points have different histories, these quantities must be updated in order to compute the history-dependent variables in the next time step. These variables are computed at discrete integration points, which normally lie inside the element. This yields to discontinuous fields and produces trouble, since the spatial gradients of these variables are required. To overcome theses difficulties, a smooth gradient field is obtained, based on the Godunov technique, which circumvents the computation of history variable gradients.

The constitutive Equation 32 in the convection phase can be written as:

$$\left.\frac{\partial \boldsymbol{\sigma}}{\partial t}\right|_{x_j^g} + \frac{\partial \boldsymbol{\sigma}}{\partial x_j^m} c_j = 0, \tag{38}$$

which needs to be integrated at each time step to update the stress from $\boldsymbol{\sigma}_{n+1}^{L}$ to $\boldsymbol{\sigma}_{n+1}$ at time t_{n+1}. As noted above, the main difficulty in Equation 38 is the stress gradient, which cannot be properly computed at the element level. In order to avoid computing gradients of the discontinuous fields, the Godunov technique is implemented here to transfer the internal variables, ρ_{n+1}^{L}, $\bar{\varepsilon}^{p^{L}}_{n+1}$ and $\boldsymbol{\sigma}_{n+1}^{L}$, from the Lagrangian mesh to the relocated mesh.

The Godunov method assumes a piecewise constant field of the solution of internal variable after the Lagrangian phase. In the finite element framework, this is the situation if one-point quadratures are employed. However, to allow for a subsequent generalization to multiple-point quadratures, the finite element can be subdivided into various sub-elements, each corresponding to the influence domain of a Gauss point [36]. Considering the scalar quantity, ψ, to be any component of the stress, $\boldsymbol{\sigma}$, or the effective plastic strain, $\bar{\varepsilon}^{p}$, the value of the internal variable, ψ_{n+1}, at time t_{n+1}, can be obtained from the Lagrangian solution, ψ_{n+1}^{L}, as:

$$\psi_{n+1} = \psi_{n+1}^{L} - \frac{\Delta t}{2A}\sum_{s=1}^{N_s}\Big\{ f_s(\psi_{n+1}^{Lc} - \psi_{n+1}^{L}) \times [1 - \alpha_0 \text{sign}(f_s)]\Big\}, \tag{39}$$

where A is the area of the sub-element, N_s the number of edges of the sub-element, and ψ_{n+1}^{Lc} is the value of ψ_{n+1}^{L} in the contiguous sub-element across edge s (Figure 5). The upwind parameter, α_0, is in the range of $0 \le \alpha_0 \le 1$, where $\alpha_0 = 1$ corresponds to a full-donor approximation and $\alpha_0 = 0$ is a centered approximation. In the above relation, f_s is the flux of the convective velocity, c, across edge s, defined as:

$$f_s = \int_s \mathbf{c}.\mathbf{n}\, ds. \tag{40}$$

Based on this approach, if, for instance, quadrilaterals with 2×2 integration points are employed, each element is divided into four sub-elements, as shown in Figure 5. In each sub-element, ψ is assumed to be constant and represented by the Gauss point value. Thus, ψ is a piecewise constant field with respect to the mesh of sub-elements, and Relation 39 can be employed to update the value of ψ for each sub-element.

THE X-ALE-FEM ANALYSIS

Application of ALE Technique into X-FEM Method

In X-ALE-FEM analysis, the X-FEM method is performed, together with an operator splitting technique, in which each time step consists of two stages: Lagrangian (material) and Eulerian (smoothing) phases. In the material phase, the X-FEM analysis is carried out based on an updated Lagrangian approach. It means that the convective terms are neglected and only material effects are considered. The time step is then followed by an Eulerian phase in which the convective term is taken into account. In this step, the nodal points move arbitrarily in the space so that the computational mesh has a regular shape and mesh

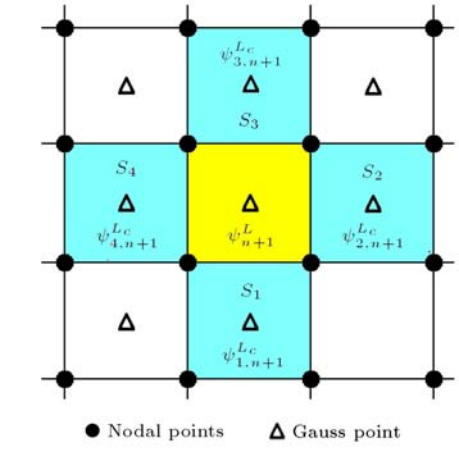

(a) One-point-quadrature

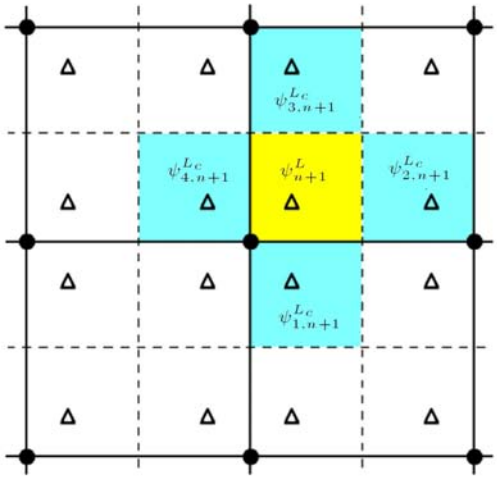

(b) Multiple-point-quadrature

Figure 5. Illustration of the Godunov technique.

distortion can be prevented. However, the material interface is independent of the FE mesh.

Figure 6 presents the mesh configuration including the material interface, before and after the Eulerian phase. In this figure, the position of the interface has been shown in two different cases. In Figure 6a, the interface does not move from one element to another during the smoothing phase. On the other hand, the number of elements which has been cut by the interface does not change during the smoothing phase, while in Figure 6b, the material interface may move from one element to another. As can be seen, elements 1, 3 and 4 have been cut by the interface before the mesh motion procedure. However, only element 3 is cut by the interface after the Eulerian phase. Thus, the number of enriched nodes may be different during the X-ALE-FEM analysis, which results in a different number of degrees-of-freedom in two successive steps. There are two main requirements that need to be considered in the smoothing phase:

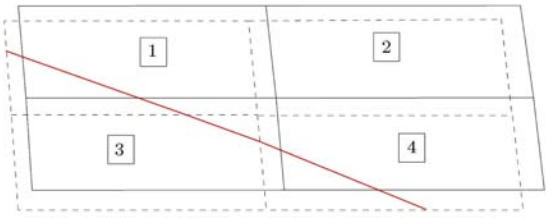

(a) The interface does not move from one element to another

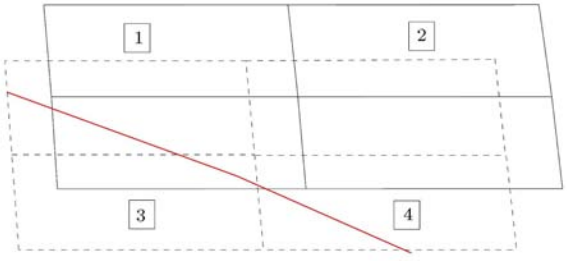

(b) The interface moves from one element to another

Figure 6. Mesh configuration before and after Eulerian phase together with the material interface in X-ALE-FEM analysis. The dashed and solid elements correspond to mesh configuration before and after mesh motion, respectively.

1. Due to the movement of nodal points in the mesh motion process, a procedure must be applied to determine the new nodal values of the level set enrichment function.
2. In the extended finite element analysis, the number of Gauss quadrature points for numerical integration of elements cut by the interface can be determined using the sub-quadrilaterals obtained by the partitioning procedure. However, in the case wherein the material interface leaves one element to another during the mesh update procedure, the number of Gauss quadrature points of an element may differ before and after mesh motion. Hence, an accurate and efficient technique must be applied into the Godunov scheme to update the stress values.

Level Set Update

During the smoothing phase, the nodal points are relocated in order to keep the computational mesh in regular shape. However, the material interface is independent of the FE mesh, as shown in Figure 7. In this figure, the dashed lines illustrate the old mesh and the relocated elements are depicted by solid lines. The aim is to obtain the level set value for node I after the Eulerian phase. For this purpose, we must determine the distance of the relocated node, I, from the interface. The intersection of the interface with the edges of old elements can be calculated at the end

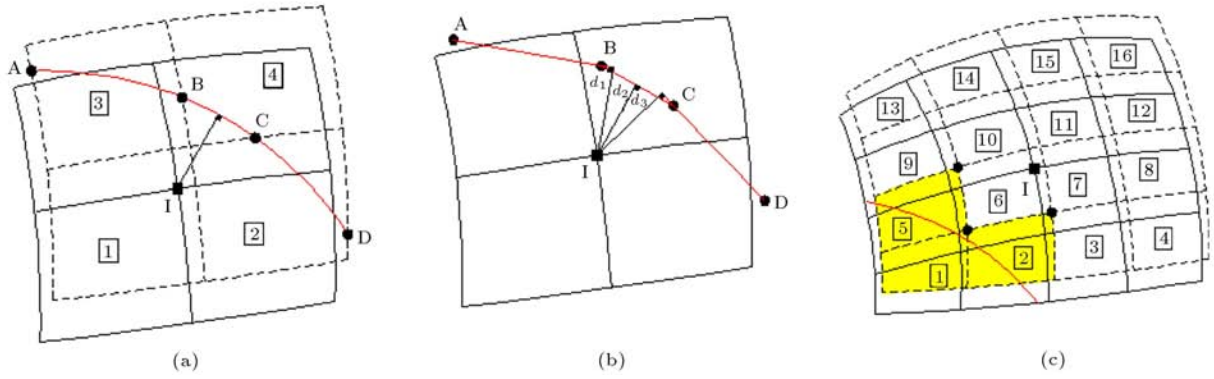

Figure 7. The procedure for determination of level set nodal values after mesh motion.

of the Lagrangian step, called points A, B, C and D in Figure 7a. The procedure used here to update the nodal values of the level set is as follows; The arc ABCD is first approximated by several straight lines that connect the intersection of the interface with the edges of old elements, i.e. lines AB, BC and CD in Figure 7b. The support domain of node I has been indicated by elements 1, 2, 3 and 4 in Figure 7a. Among the elements of the support domain, we define the Extended Support Domain (ESD) of node I that contains those elements cut by the interface at the end of the Lagrangian phase. As can be seen from Figure 7b, the ESD of node I includes elements 2, 3 and 4. For each element of ESD, the distance of the relocated node, I, is calculated from the element interface. The exact value of the level set function for the relocated node, I, is the minimum value of distances, d_1, d_2 and d_3, as shown in Figure 7b. In order to determine the sign of the level set value for the relocated node, I, the above procedure will be performed once again to evaluate the value of the level set for the old node, I. If the sign of these two level set values are similar, it means that the old and relocated nodes lie in the same side of the interface. Thus, the sign of the level set value for the relocated node I must be identical with its sign for the old node I.

However, the proposed algorithm is not appropriate for determination of the level set value of nodal points that are not enriched during the Lagrangian phase, and included in an element split by the interface after mesh motion (e.g. node I in Figure 7c). In this case, the ESD of node I in Figure 7c contains no elements, and the definition of ESD must be modified. In order to modify the ESD for these nodal points, we first indicate the support domain of node I (e.g. elements 6, 7, 10 and 11 in Figure 7c). All nodal points of this domain, which were enriched during the Lagrangian phase, are selected (circled nodes in Figure 7c). Those elements in the union of circled nodes' support domains that are cut by the interface can be considered as the modified ESD of node I. The procedure will be then followed by determination of the level set value for node I, as demonstrated above. By substituting the nodal values of the level set in Equation 2, the level set function can be finally expressed. The iso-zero of the level set function determines the location of the interface.

Stress Update and Numerical Integration

A key point of the Godunov-like stress update procedure is that the number of Gauss points before and after mesh motion must be equal. In addition, the natural coordinates of Gauss quadrature points must remain constant during the smoothing phase. However, these conditions may not be necessarily satisfied in the Eulerian phase of an X-ALE-FEM analysis, since the elements cut by the interface are divided into sub-polygons whose Gauss points are used for numerical integration. It must be noted that for the elements cut by the interface boundary, the standard Gauss quadrature points are insufficient for numerical integration, and may not adequately integrate the interface boundary. Thus, it is necessary to modify the element quadrature points to accurately evaluate the contribution to the weak form for both sides of the interface. In the standard FE method, numerical integration can be performed by discretizing the domain, as $\Omega = \bigcup_{e=1}^{m} \Omega_e$ in which m is the number of elements and Ω_e is the element sub-domain. In X-FEM, the elements located on the interface boundary can be partitioned by sub-polygons, Ω_s, with the boundaries aligned with the material interface, i.e. $\Omega_e = \bigcup_{s=1}^{m_s} \Omega_s$ in which m_s denotes the number of sub-polygons of the element. It is important that the Gauss points of sub-polygons are only used for numerical integration of the elements cut by the interface and no new degrees of freedom are added to system. Different algorithms may be applied to generate these sub-polygons, based on sub-triangles and sub-quadratics. However, for the following two

reasons, the sub-triangles are not suitable in an X-ALE-FEM analysis:

a) Due to the relative motion between the interface and elements, the natural coordinates of Gauss quadrature points may differ during the smoothing phase, even though the interface does not leave the element to another in this phase,

b) During the evolution of relative motion between the interface and nodal points, it is possible that a nodal point lies close to the interface. In this case, partitioning the bounded part between the node and the interface by sub-triangles results in serious numerical errors.

Thus, the numerical integration of elements cut by the interface is performed here based on sub-quadrilaterals, as shown in Figure 8. In this technique, it is not necessary for the sub-quadrilaterals to conform to the geometry of the interface. However, it is required to have enough sub-divisions to reduce the errors of numerical integration. Considering each split element contains 8×8 subdivisions, the total number of Gauss points is 64 for each split element, while, in standard elements, a set of 2×2 Gauss points are used for numerical integration. Based on the sub-quadrilaterals integration scheme, the natural coordinates of Gauss quadrature points are independent of the interface position and do not change during the smoothing phase. Furthermore, the most important feature is that the error of numerical integration can be significantly reduced in this technique. However, a key requirement of the Godunov scheme is the equivalence of integration points before and after the mesh update process that are not satisfied in the Eulerian phase of an X-ALE-FEM analysis when the interface leaves one element to another, or moves into the relocated element during the smoothing procedure. In this circumstance, four different cases may occur regarding the number of Gauss quadrature points:

1. The element is not cut by the interface either before or after mesh motion (e.g. elements 1, 2, 3 and 7 in Figures 9a and 9b). In this case, the FE standard Gauss points are used for numerical integration before and after the smoothing phase. Thus, the number of Gauss points and their natural coordinates remain constant, and the Godunov scheme can be used without any modification.

2. The element which has been cut by the interface before the smoothing phase is still cut by the interface after the mesh updating procedure (e.g. elements 4, 5 and 9 in Figures 9a and 9b). Based on the new integration scheme, both the old and relocated elements contain 64 Gauss quadrature points, and the natural coordinates of Gauss points do not change. Hence, the Godunov scheme can be applied without any modification.

3. The interface leaves one element for another during the smoothing phase. In this case, the element which was split by the interface before the mesh updating procedure does not contain the interface after mesh motion (e.g. element 6 in Figures 9a and 9b). It, therefore, results in different numbers of Gauss points in the old and relocated elements. As mentioned earlier, the old and relocated elements contain 64 and 4 Gauss quadrature points, respectively. Thus, an efficient algorithm must be applied into the Godunov technique to update the stress from $\boldsymbol{\sigma}_{n+1}^{L}$ obtained from the Lagrangian phase to $\boldsymbol{\sigma}_{n+1}$ after the Eulerian phase. First, the internal variables such as stresses are updated from the 8×8 Gauss points in the old element to a virtual set of 8×8 FE standard Gauss points in the relocated mesh via a Godunov update algorithm. The stress values must be then transferred from the virtual Gauss points to relocated 2×2 Gauss points

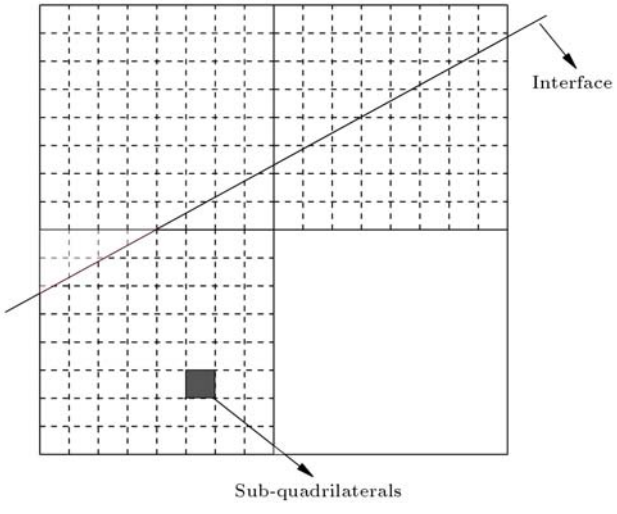

Figure 8. The sub-quadrilateral partitioning for numerical integration of elements cut by the interface.

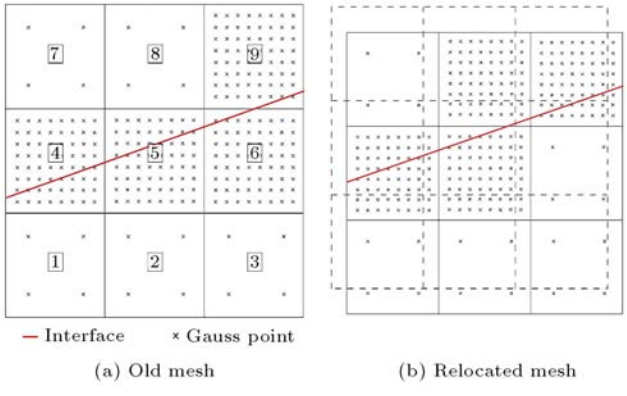

Figure 9. The distribution of Gauss integration points in the X-ALE-FEM analysis.

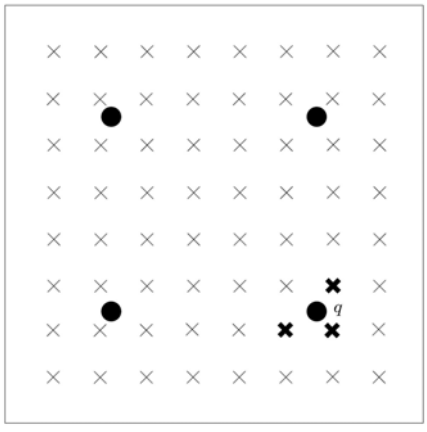

Figure 10. The support domain of Gauss integration point q; •: The Gauss points 2×2 corresponding to relocated mesh, ×: The virtual Gauss points in relocated mesh.

in the updated element, as shown in Figure 10. According to this figure, for each FE Gauss point, q, there is a support domain which consists of the three nearest virtual Gauss points. The stress value at q can be interpolated from the stress values of these three nearest Gauss points.

4. The material interface moves into the relocated element during the Eulerian phase. In this case, the relocated element is cut by the interface, while it was not included before the mesh motion (e.g. element 8 in Figures 9a and 9b). In this case, the stress values have been calculated at the 2×2 standard FE Gauss points of the old element at the end of the Lagrangian phase. These values must be updated using the Godunov algorithm to obtain the stress values at the virtual 2×2 Gauss points in the relocated element. It must be noted that the stress values are required at relocated 8×8 Gauss quadrature points. For this aim, the stress values are firstly computed at the nodal points of the relocated element by using an averaging technique from the related values at the nearest Gauss points. The required stress values at relocated 8×8 Gauss points can be then obtained using the standard FE shape functions of relocated nodal values.

NUMERICAL SIMULATION RESULTS

In order to illustrate the applicability of the proposed computational algorithm in large elasto-plastic deformation problems, several numerical examples are presented, including the coining problem with horizontal and vertical moving boundaries and a tensile plate with a moving interface. The examples are solved using FEM, X-FEM and X-ALE-FEM techniques, and the results are compared. The initial mesh used for X-FEM and X-ALE-FEM methods are similar and independent of the discontinuity shape, while, in FEM analysis, the FE mesh needs to be conformed to the geometry of discontinuity. In order to perform a real comparison, the number of elements in FEM and X-FEM analyses is almost equal. All examples are simulated by a plain strain representation and the convergence tolerance is set to 5×10^{-14}.

Coining Test

The first example illustrates the performance of the X-ALE-FEM technique in large deformation simulation of a practical and challenging example, extensively used to present the performance of the ALE technique in literature. The proposed technique is implemented to simulate the coining problem by pressing a rigid component into the flexible elastic foam. Two different cases are considered in analysis of the current example, including the horizontal and vertical moving boundaries.

In the first case, the coining problem is assumed with a horizontal moving boundary, while the edge of the component is restrained at the right-hand side, as shown in Figure 11. The geometry and boundary conditions together with the problem definition are shown in this figure. An elasto-plastic metallic component of von-Mises behavior with the Young modulus of 2.1×10^6 kg/cm^2, Poisson coefficient of 0.35, a yield stress of 2400 kg/cm^2 and a hardening parameter of 3.0×10^3 kg/cm^2 is pressed from the bottom edge into the elastic foam with the Young modulus of 2.1×10^5 kg/cm^2 and Poisson coefficient of 0.35. The component is restrained at the top edge along the line, BG, and all contact surfaces, AC, CF, DF, are frictionless. In Figure 12, the FEM and X-ALE-FEM meshes are shown together with the material interface, at the initial stage of compaction. For both simulations, the material interface conforms to the edge of elements at the initial configuration, in order to

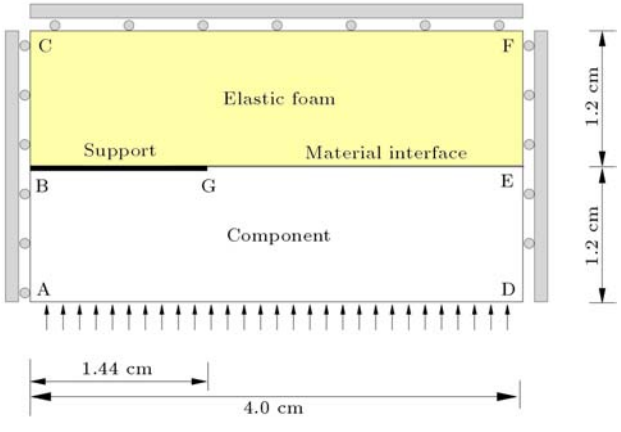

Figure 11. Coining test with a horizontal interface; Problem definition.

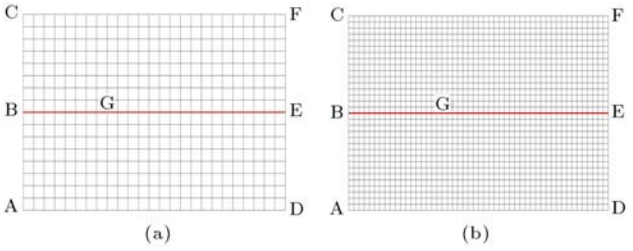

Figure 12. Coining test with a horizontal interface; the FEM and X-ALE-FEM meshes of (a) 400 elements, (b) 1600 elements.

simplify the implementation of displacement boundary conditions along the edge, BG. However, the movement of interface GE is independent of the grid in X-ALE-FEM analysis as the compaction proceeds. It must be noted that the X-FEM analysis leads to similar results obtained by FEM modeling as the interface passes through the nodal points. The simulation of this example poses a major difficulty using the Lagrangian formulation due to highly distorted mesh, particularly around point G; aborting the calculations and causing numerical errors at the compaction of 0.7 cm.

In Figures 13a and 13c, the deformed finite element meshes are shown for fine mesh at the pressing of 0.35 and 0.7 cm. Based on a simple ALE remeshing strategy with the equal height and width of elements prescribed in the regions of ABED and BCFE, the X-ALE-FEM analysis can be performed until 0.83 cm height reduction. The deformed X-ALE-FEM configuration for fine mesh is presented in Figures 13b, 13d and 13e corresponding to the compaction deformations of 0.35, 0.7 and 0.83 cm. The contours of normal stress, $\boldsymbol{\sigma}_y$ distribution of the component are shown in Figure 14 for both FEM and X-ALE-FEM methods at the height reduction of 0.5 cm. Remarkable agreements can be observed between two different techniques. A comparison has been performed using two techniques by evolution of the vertical reaction and vertical displacement of point E with compaction deformation in Figures 15 and 16. Good agreement can be seen up to the compaction of 0.70 cm (the final compaction obtained by the FEM analysis) using the FEM and X-ALE-FEM techniques.

In the second simulation, the coining problem is modeled with horizontal and vertical moving boundaries, as shown in Figure 17. The geometry and boundary conditions are shown together with the problem definition in this figure. Similar to previous simulation, the movement of the component is constrained along the line, BG, and the contact surfaces, AC, CF and DF, are assumed to be frictionless. Figure 18 presents the computational meshes corresponding to FEM and X-ALE-FEM analyses, together with the internal material interface at the initial stage of pressing. In order to simply implement the displacement boundary

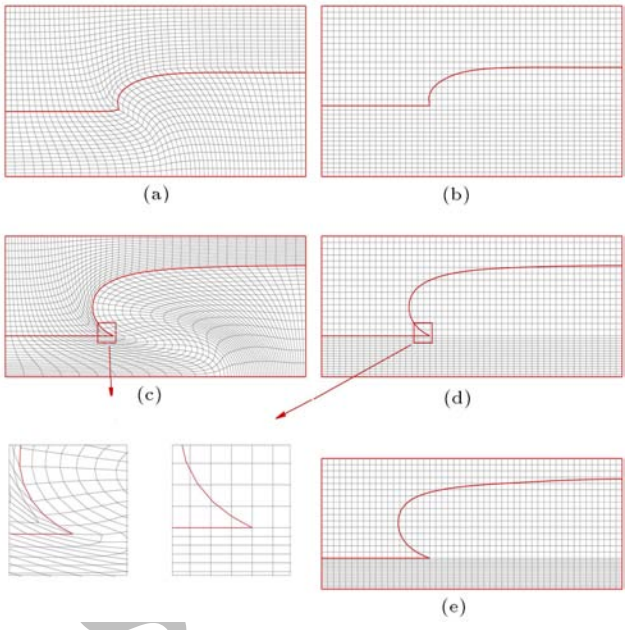

Figure 13. Coining test with a horizontal interface; the deformed configuration using fine meshes. (a) The FEM at $d = 0.35$ cm; (b) The X-ALE-FEM at $d = 0.35$ cm; (c) The FEM at $d = 0.7$ cm; (d) The X-ALE-FEM at $d = 0.7$ cm; and (e) The X-ALE-FEM at $d = 0.83$ cm

conditions along edge BG, the internal interface for both simulations coincides with the edge of elements at the initial configuration. Due to the high distortion and elongation of elements, particularly around the corners, the FE analysis aborts at 0.66 cm height reduction. However, the X-ALE-FEM analysis continues pressing until 0.816 cm by using a mesh smoothing strategy. In Figures 19a to 19d, the deformed FEM and X-ALE-FEM configurations are shown for fine mesh at die-pressing of 0.33 and 0.66 cm. Also, depicted in Figure 19e is the final deformed configuration of X-ALE-FEM mesh at 0.816 cm height reduction. In order to perform a comparison between the FEM and X-ALE-FEM results, the normal stress contours are illustrated in Figure 20 for both techniques at the pressing of 0.5 cm. In Figures 21 and 22, the variations of the reaction force and horizontal displacement of point H are shown with vertical displacement. This example clearly shows that the proposed X-ALE-FEM method can be efficiently used to model large elasto-plastic deformations in solid mechanic problems.

Plate in Tension

The next example is of a rectangular plate under uniaxial extension up to an elongation of 6.4 cm, as shown in Figure 23. The plate has an elasto-plastic von-Mises behavior with the Young modulus of 2.1×10^6 kg/cm^2, Poisson coefficient of 0.35, yield stress of 2400 kg/cm^2 and a hardening parameter of 100 kg/cm^2. The

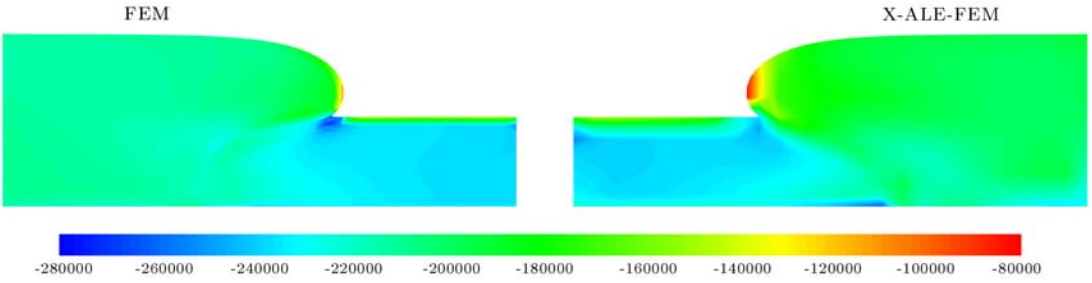

Figure 14. Coining test with a horizontal interface; the normal stress σ_y contours of rigid part at $d = 0.5$ cm; a comparison between FEM and X-ALE-FEM analyses.

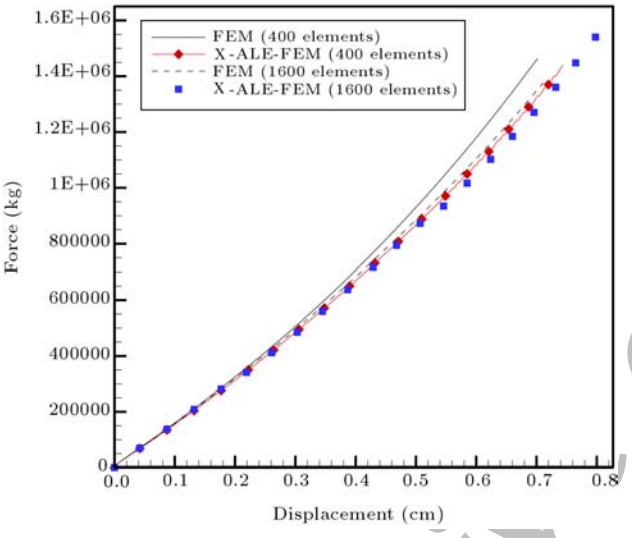

Figure 15. Coining test with a horizontal interface; the variation of reaction force with vertical displacement; a comparison between FEM and X-ALE-FEM analyses.

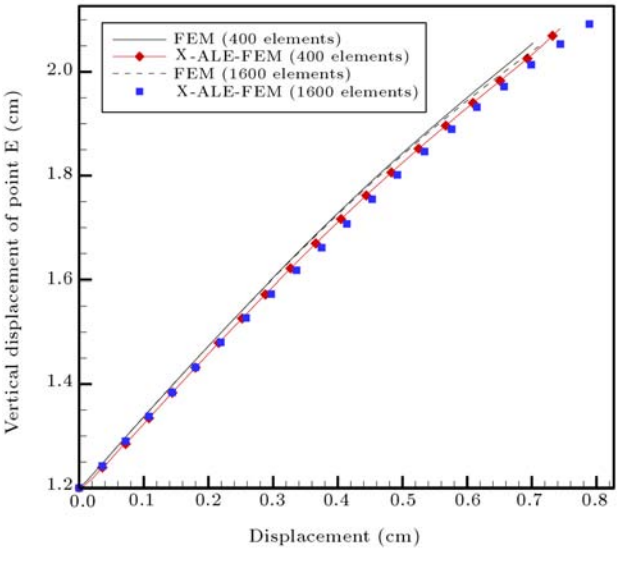

Figure 16. Coining test with a horizontal interface; the variation of vertical displacement of point E with displacement; a comparison between FEM and X-ALE-FEM analyses.

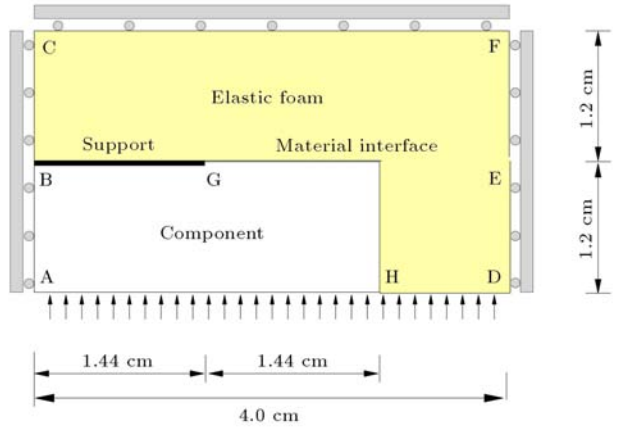

Figure 17. Coining test with a horizontal and vertical interfaces; problem definition.

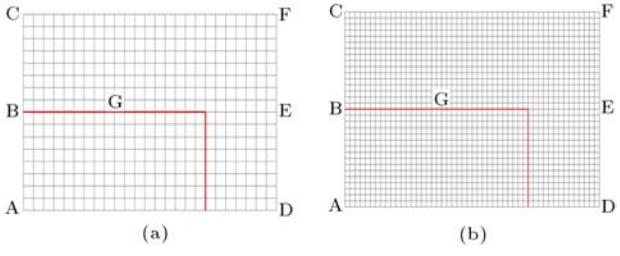

Figure 18. Coining test with a horizontal and vertical interfaces; the FEM and X-ALE-FEM meshes of (a) 400 elements and (b) 1600 elements.

necking may be physically occurred at each part of the specimen. In order to control the phenomenon, a geometric imperfection of 1% reduction in width is induced in the central part of the plate. On the virtue of symmetry, only one-quarter of the metallic plate is modeled under a plane strain condition (Figure 23a). The analysis is performed using the FEM, X-FEM and X-ALE-FEM techniques and the results are compared. In order to make a comprehensive comparison, the FEM analysis is carried out using both the Lagrangian and ALE approaches.

The finite element mesh has 480 linear quadrilateral elements, as shown in Figure 23b. In order

to demonstrate the performance of X-FEM and X-ALE-FEM methods in modeling discontinuities, due to the significant difference of material properties, the numerical simulation is performed using a metallic part, whose geometry and properties are similar to the FE model connected to a rectangular part with zero Young modulus. Figure 23c illustrates the X-FEM and X-ALE-FEM meshes of 600 uniform elements, together with the geometry of the model. The boundary conditions are applied by restricting the bottom edge in y-direction and the left edge in x-direction. In the X-FEM and X-ALE-FEM models, all nodal points of the right edge are restrained in a x-direction.

A very simple remeshing strategy is applied for

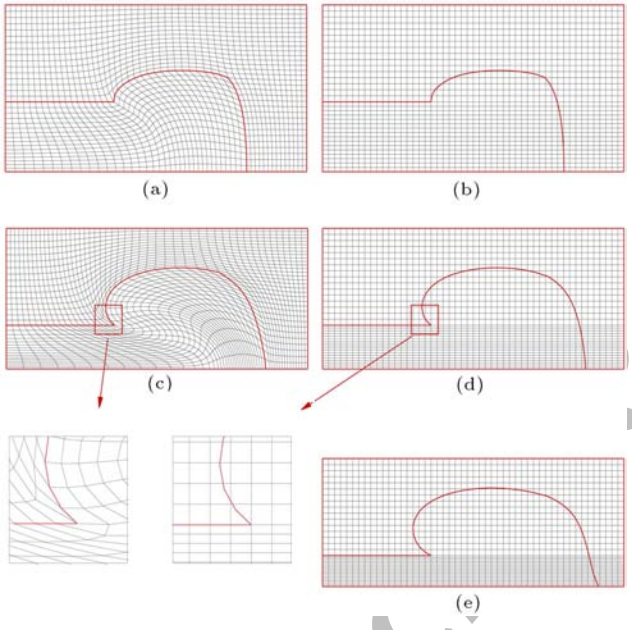

Figure 19. Coining test with a horizontal and vertical interfaces; the deformed configuration using fine meshes. (a) The FEM at $d = 0.33$ cm; (b) The X-ALE-FEM at $d = 0.33$ cm; (c) The FEM at $d = 0.66$ cm; (d) The X-ALE-FEM at $d = 0.66$ cm; and (e) The X-ALE-FEM at $d = 0.816$ cm

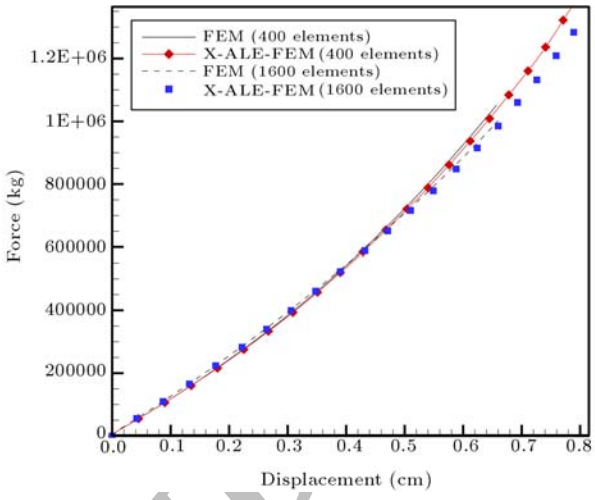

Figure 21. Coining test with a horizontal and vertical interfaces; the variation of reaction force with vertical displacement; a comparison between FEM and X-ALE-FEM analyses.

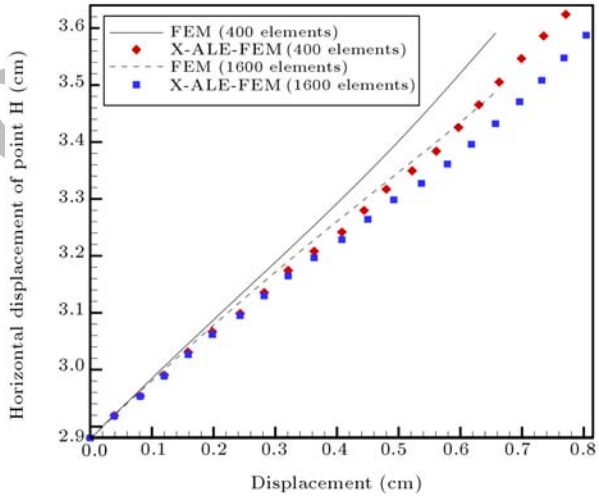

Figure 22. Coining test with a horizontal and vertical interfaces; the variation of horizontal displacement of point H with vertical displacement; a comparison between FEM and X-ALE-FEM analyses.

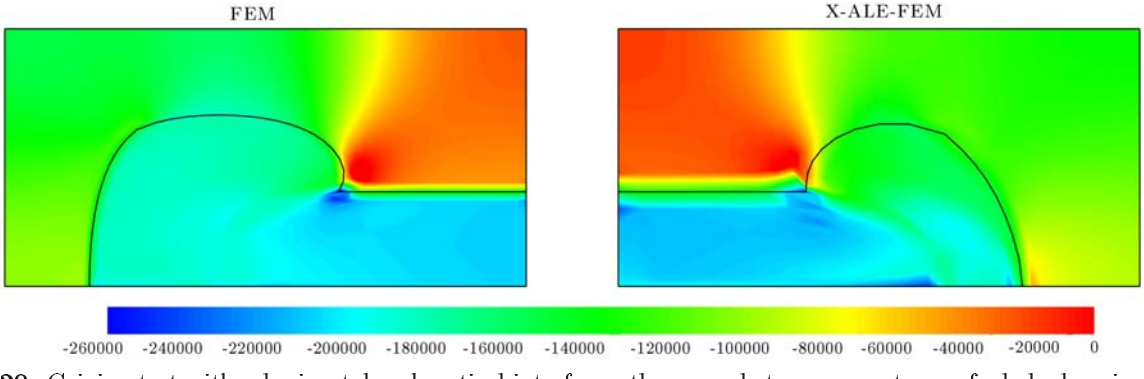

Figure 20. Coining test with a horizontal and vertical interfaces; the normal stress σ_y contours of whole domain at $d = 0.5$ cm; a comparison between FEM and X-ALE-FEM analyses.

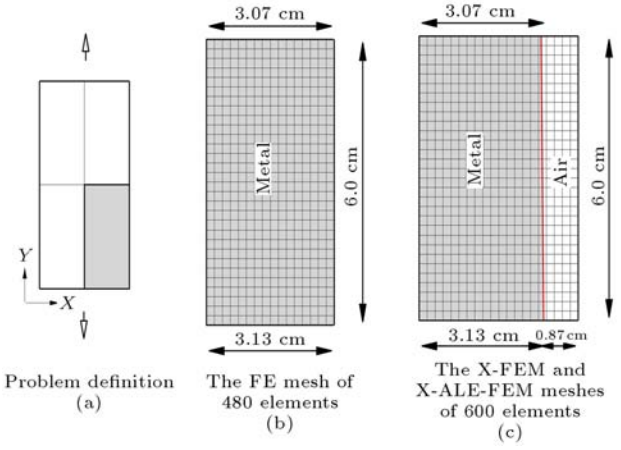

Figure 23. A plate in tension.

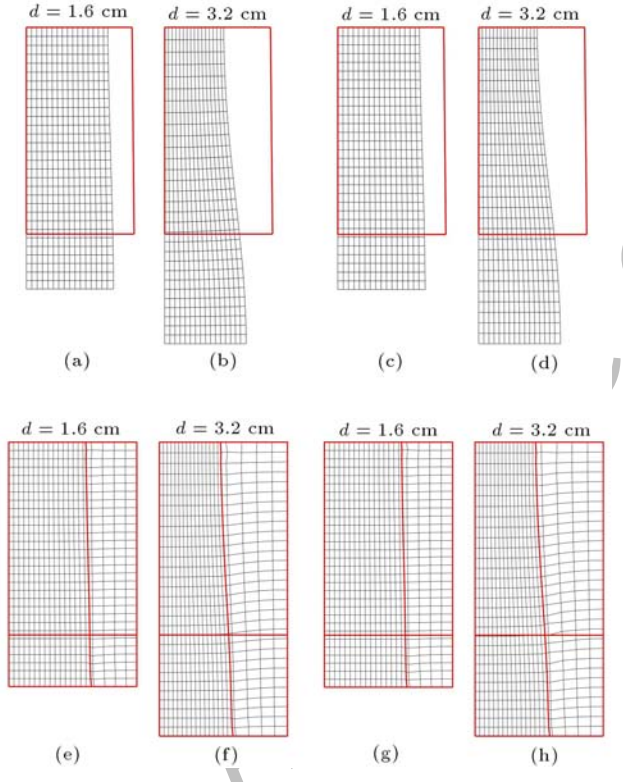

Figure 24. A plate in tension; the mesh configurations at different bottom displacements. (a-b) Lagrangian formulation, (c-d) ALE formulation, (e-f) X-FEM formulation, (g-h) X-ALE-FEM formulation.

the ALE analysis, in which the equal height of elements is prescribed in the whole domain. The Laplacian approach is used in the X-ALE-FEM analysis to reduce the mesh distortion and produce a smooth mesh. Figure 24 presents the deformed configuration obtained by four techniques, i.e. the Lagrangian approach, the ALE, X-FEM and X-ALE-FEM methods, up to an elongation of 3.2 cm for one quarter of the specimen. The variations of normal stress, σ_y, along the vertical symmetry plane are shown in Figure 25 at the half

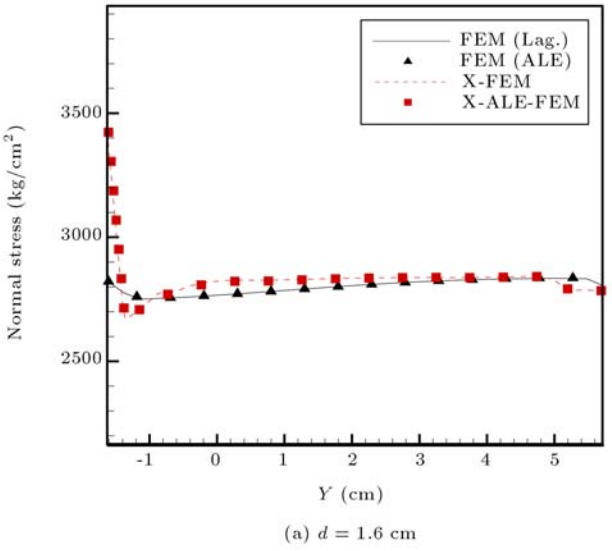

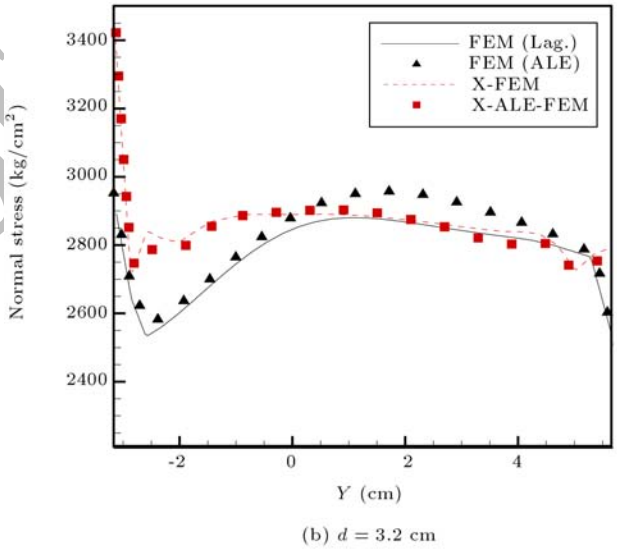

Figure 25. A plate in tension; a comparison of normal stress between the FEM, X-FEM and X-ALE-FEM techniques; the stress σ_y distribution along vertical symmetry plane.

and final stages of the tensile process for four different techniques. In Figure 26, a quantitative comparison is performed between various methods by evolution of the vertical reaction at different vertical displacements. The variation of dimensionless width (ratio of current to initial width) at the necking section is illustrated with elongation in Figure 27. Obviously, it can be concluded that the proposed X-ALE-FEM method can be successfully used to model large deformations in elasto-plastic behavior.

CONCLUSION

In the present paper, a new computational technique was presented for the modeling of moving boundaries

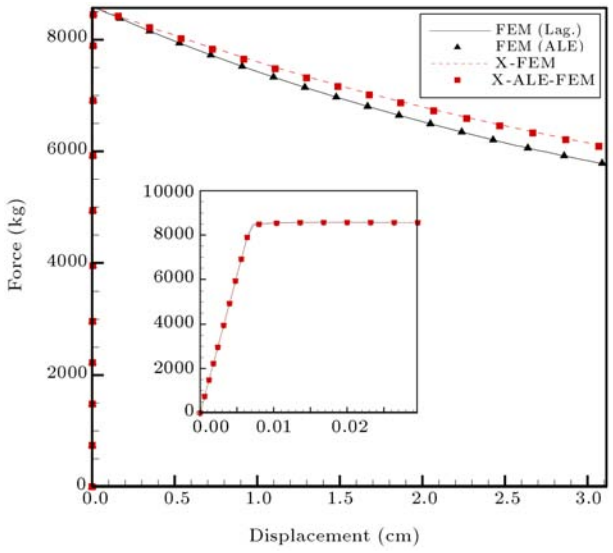

Figure 26. A plate in tension; the variation of reaction force with vertical displacement; a comparison between FEM, X-FEM and X-ALE-FEM analyses.

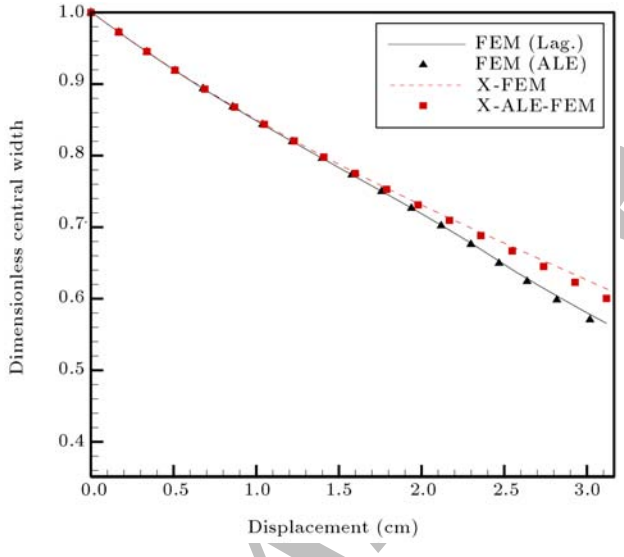

Figure 27. A plate in tension; the dimensionless width at the necking section versus the edge displacement; a comparison between FEM, X-FEM and X-ALE-FEM analyses.

in large plastic deformations based on an enriched arbitrary Lagrangian-Eulerian finite element method. The X-FEM method was developed in the framework of an arbitrary Lagrangian-Eulerian formulation for the large deformation of solid mechanic problems by implementation of the enrichment functions to approximate the displacement fields of elements located on discontinuity due to different material properties. The X-FEM method was applied by performing a splitting operator to separate the material (Lagrangian) phase from the convective (Eulerian) phase. The Lagrangian phase was carried out by partitioning the domain with sub-quadrilaterals whose Gauss points were used for integration of the domain of the elements. The ALE governing equation was derived by substituting the relationship between the material time derivative and grid time derivative into the governing equations of continuum mechanics. The analysis was carried out according to the Lagrangian phase at each time step until the required convergence was attained. The Eulerian phase was then applied to keep the mesh configuration regular. In the Eulerian phase, the nodal points were relocated arbitrarily, and the material interface was independent of the FE mesh. A technique was proposed to update the nodal values of the level set and the natural coordinate of Gauss quadrature points, which could be different before and after the mesh updating procedure. Furthermore, a technique was applied to update the stress values from the old Gauss points to the new ones based on the Godunov stress updating scheme. Finally, the applicability of the proposed X-ALE-FEM method was demonstrated through several numerical examples of large deformation processes including the coining problem with horizontal and vertical moving boundaries and a tensile plate with moving interface. The results are compared with those of classical finite element and extended finite element methods. It was shown that the X-ALE-FEM technique can be used efficiently to prevent the grid from severe mesh distortion, and model the large plasticity deformation in continuum mechanic problems.

REFERENCES

1. Melenk, J.M. and Babuska, I. "The partition of unity finite element method: Basic theory and applications", *Comp. Meth. Appl. Mech. Engng.*, **139**, pp. 289-314 (1996).
2. Dolbow, J.E. "An extended finite element method with discontinuous enrichment for applied mechanics", Ph.D. Thesis, Northwestern University (1999).
3. Belytschko, T. and Black, T. "Elastic crack growth in finite elements with minimal remeshing", *Int. J. Numer. Meth. Engng.*, **45**, pp. 601-620 (1999).
4. Moës, N., Dolbow, J.E. and Belytschko, T. "A finite element method for crack growth without remeshing", *Int. J. Numer. Meth. Engng.*, **46**, pp. 131-150 (1999).
5. Dolbow, J., Moës, N. and Belytschko, T. "An extended finite element method for modeling crack growth with frictional contact", *Comp. Meth. Appl. Mech. Engng.*, **190**, pp. 6825-6846 (2001).
6. Sukumar, N., Chopp, D.L., Moës, N. and Belytschko, T. "Modeling holes and inclusions by level sets in the extended finite-element method", *Comp. Meth. Appl. Mech. Engng.*, **190**, pp. 6183-6200 (2001).
7. Belytschko, T., Moës, N., Usui, S. and Parimi, C. "Arbitrary discontinuities in finite elements", *Int. J. Numer. Meth. Engng.*, **50**, pp. 993-1013 (2001).

8. Stolarska, M., Chopp, D.L., Moës, N. and Belytschko, T. "Modeling crack growth by level sets in the extended finite element method", *Int. J. Numer. Meth. Engng.*, **51**, pp. 943-960 (2001).
9. Moës, N. and Belytschko, T. "Extended finite element method for cohesive crack growth", *Engng. Fract. Mech.*, **69**, pp. 813-833 (2002).
10. Sukumar, N. and Prévost, J.H. "Modeling quasi-static crack growth with the extended finite element method. Part I: Computer implementation", *Int. J. Solids Struct.*, **40**, pp. 7513-7537 (2003).
11. Ventura, G., Budyn, E. and Belytschko, T. "Vector level sets for description of propagating cracks in finite elements", *Int. J. Numer. Meth. Engng.*, **58**, pp. 1571-1592 (2003).
12. Wagner, G.J., Moës, N., Liu, W.K. and Belytschko, T. "The extended finite element method for stokes flow past rigid cylinders", *Int. J. Numer. Meth. Engng.*, **51**, pp. 393-413 (2001).
13. Moës, N., Cloirec, M., Cartraud, P. and Remacle, J.F. "A computational approach to handle complex microstructure geometries", *Comp. Meth. Appl. Mech. Engng.*, **192**, pp. 3163-3177 (2003).
14. Chessa, J. and Belytschko, T. "An enriched finite element method and level sets for axisymmetric two-phase flow with surface tension", *Int. J. Numer. Meth. Engng.*, **58**, pp. 2041-2064 (2003).
15. Chessa, J. and Belytschko, T. "Arbitrary discontinuities in space-time finite elements by level sets and X-FEM", *Int. J. Numer. Meth. Engng.*, **61**, pp. 2595-2614 (2004).
16. Lee, S.H., Song, J.H., Yoon, Y.C., Zi, G. and Belytschko, T. "Combined extended and superimposed finite element method for cracks", *Int. J. Numer. Meth. Engng.*, **59**, pp. 1119-1136 (2004).
17. Sukumar, N., Huang, Z.Y., Prévost, J.H. and Suo, Z. "Partition of unity enrichment for bimaterial interface cracks", *Int. J. Numer. Meth. Engng.*, **59**, pp. 1075-1102 (2004).
18. Patzák, B. and Jirásek, M. "Process zone resolution by extended finite elements", *Engng Fract. Mech.*, **70**, pp. 957-977 (2003).
19. Legay, A., Wang, H.W. and Belytschko, T. "Strong and weak arbitrary discontinuities in spectral finite elements", *Int. J. Numer. Meth. Engng.*, **64**, pp. 991-1008 (2005).
20. Khoei, A.R. and Nikbakht, M. "An enriched finite element algorithm for numerical computation of contact friction problems", *Int. J. Mech. Sciences.*, **49**, pp. 183-199 (2007).
21. Kim, T.Y., Dolbow, J. and Laursen, T. "A mortared finite element method for frictional contact on arbitrary interfaces", *Comput. Mech.*, **39**, pp. 223-236 (2007).
22. Khoei, A.R., Shamloo, A. and Azami, A.R. "Extended finite element method in plasticity forming of powder compaction with contact friction", *Int. J. Solids Struct.*, **43**, pp. 5421-5448 (2006).
23. Anahid, M. and Khoei, A.R. "New development in extended finite element modeling of large elasto-plastic deformations", *Int. J. Numer. Meth. Engng.*, **75**, pp. 1133-1171 (2008).
24. Khoei, A.R., Biabanaki, S.O.R. and Anahid, M. "Extended finite element method for three-dimensional large plasticity deformations", *Computer Methods in Applied Mechanics and Engineering*, **197**, pp. 1100-1114 (2008).
25. Lewis, R.W. and Khoei, A.R. "Numerical modeling of large deformation in metal powder forming", *Comp. Meth. Appl. Mech. Engng.*, **159**, pp. 291-328 (1998).
26. Khoei, A.R. and Lewis, R.W. "Adaptive finite element remeshing in a large deformation analysis of metal powder forming", *Int. J. Numer. Meth. Engng.*, **45**, pp. 801-820 (1999).
27. Khoei, A.R. and Gharehbaghi, S.A. "Three-dimensional data transfer operators in plasticity using SPR technique with C_0, C_1 and C_2 continuity", *Scientia Iranica*, **15**(5), pp. 554-567 (2008).
28. Haber, R.B. "A mixed Eulerian-Lagrangian displacement model for large-deformation analysis in solid mechanics", *Comp. Meth. Appl. Mech. Engng.*, **43**, pp. 277-292 (1984).
29. Liu, W.K., Belytschko, T. and Chang, H. "An Arbitrary Lagrangian-Eulerian finite element method for path-dependent materials", *Comp. Meth. Appl. Mech. Engng.*, **58**, pp. 227-245 (1986).
30. Liu, W.K., Chang, H., Chen, J.S., Belytschko, T. and Zhang, Y.F. "Arbitrary Lagrangian-Eulerian Petrov-Galerkin finite elements for nonlinear continua", *Comp. Meth. Appl. Mech. Engng.*, **68**, pp. 259-310 (1988).
31. Benson, D.J. "An efficient, accurate, simple ALE method for nonlinear FE programs", *Comp. Meth. Appl. Mech. Engng.*, **72**, pp. 305-350 (1989).
32. Yamada, T. and Kikuchi, F. "An arbitrary Lagrangian-Eulerian finite element method for incompressible hyperelasticity", *Comp. Meth. Appl. Mech. Engng.*, **102**, pp. 149-177 (1993).
33. Ghosh, S. and Raju, S. "$R-S$ adapted arbitrary Lagrangian-Eulerian finite element method of metal-forming with strain localization", *Int. J. Numer. Meth. Engng.*, **39**, pp. 3247-3272 (1996).
34. Wang, J. and Gadala, M.S. "Formulation and survey of ALE method in nonlinear solid mechanics", *Finite Elem. Anal. Design*, **24**, pp. 253-269 (1997).
35. Gadala, M.S. and Wang, J. "ALE formulation and its application in solid mechanics", *Comp. Meth. Appl. Mech. Engng.*, **167**, pp. 33-55 (1998).
36. Rodriguez-Ferran, A., Casadei, F. and Huerta, A. "ALE stress update for transient and quasistatic processes", *Int. J. Numer. Meth. Engng.*, **43**, pp. 241-262 (1998).
37. Rodriguez-Ferran, A., Perez-Foguet, A. and Huerta, A. "Arbitrary Lagrangian-Eulerian (ALE) formulation for

hyperelastoplasticity", *Int. J. Numer. Meth. Engng.*, **53**, pp. 1831-1851 (2002).

38. Armero, F. and Love, E. "An arbitrary Lagrangian-Eulerian finite element method for finite strain plasticity", *Int. J. Numer. Meth. Engng.*, **57**, pp. 471-508 (2003).
39. Bayoumi, H.N. and Gadala, M.S. "A complete finite element treatment for the fully coupled implicit ALE formulation", *Comput. Mech.*, **33**, pp. 435-452 (2004).
40. Khoei, A.R., Azami, A.R., Anahid, M. and Lewis, R.W. "A three-invariant hardening plasticity for numerical simulation of powder forming processes via the arbitrary Lagrangian-Eulerian FE model", *Int. J. Numer. Meth. Engng.*, **66**, pp. 843-877 (2006).
41. Khoei, A.R., Anahid, M., Shahim, K. and DorMohammadi, H. "Arbitrary Lagrangian-Eulerian method in plasticity of pressure-sensitive material with reference to powder forming processes", *Comput. Mech.*, **42**, pp. 13-38 (2008).
42. Khoei, A.R., Anahid, M. and Shahim, K. "An extended arbitrary Lagrangian-Eulerian finite element method for large deformation of solid mechanics", *Finite Elem. Anal. Design*, **44**, pp. 401-416 (2008).
43. Sethian, J.A., *Level Set Methods and Fast Marching Methods: Evolving Interfaces in Computational Geometry, Fluid Mechanics, Computer Vision, and Material Science*, Cambridge University Press (1999).
44. Belytschko, T., Liu, W.K. and Moran, B., *Nonlinear Finite Elements for Continua and Structures*, Wiley (2000).
45. Herrmann, L.R. "Laplacian-isoparametric grid generation scheme", *ASCE Engng. Mech. Div.*, **102**, pp. 749-756 (1976).

BIOGRAPHIES

M. Anahid completed his BS, MS and PhD studies in the civil engineering department at Sharif University of Technology in 2007. After PhD graduation, he was appointed as a Postdoctoral Researcher in the mechanical engineering department at Ohio State University, where he is currently a Research Associate.

A.R. Khoei received his PhD in civil engineering from the University of Wales, Swansea, in the UK, in 1998. He is currently a professor in the civil engineering department at Sharif University of Technology in Iran. He is the editor of Scientica Iranica, Transaction A, Journal of Civil Engineering, a member of the editorial board of the Journal of Science and Technology (Sharif University of Technology), and the co-editor of the '11th International Symposium on Plasticity and Its Current Application in the US', 2005. Dr Khoei was selected as a distinguished researcher at Sharif University of Technology in 2003, 2005, 2007 and 2008, and as a distinguished professor by the Ministry of Science, Research and Technology in 2008. He is the silver medal winner of the Khwarizmi International Award (2005), organized by the Iranian Research Organization for Science and Technology.